

# Numerical Predictions of the Stability of a Melt Spinning Puddle

Markus Bussmann and Forhad Ahmed

Department of Mechanical and Industrial Engineering, University of Toronto, Toronto, ON M5S3G8 Canada

Email: [bussmann@mie.utoronto.ca](mailto:bussmann@mie.utoronto.ca)

## ABSTRACT

Most previous modelling of the planar flow casting process has specified a melt inflow rate into the gap between nozzle and wheel, rather than the actual boundary condition which is an applied overpressure inside the crucible. The resulting simplification typically leads to predictions of the formation of steady so-called puddles, where experimental results clearly point to a limited window of operability outside of which a stable puddle will not form. In this paper, we present details of a two-dimensional model of the flow, heat transfer, and phase change of the planar flow casting process, with applied pressure as the inlet boundary condition. The results of various simulations are then presented, that demonstrate a limited range of overpressures for a given wheel speed within which a stable puddle can be formed. On the other hand, for a given overpressure, simulations corresponding to a very wide range of wheel speed all predict stable puddles. A reason for this may be that the high wheel speed instability is a three-dimensional one, that acts across the puddle and ribbon, and so cannot be predicted by a two-dimensional model.

## 1 INTRODUCTION

Planar flow casting, also referred to as *melt spinning*, is a rapid solidification process often utilized to produce amorphous metallic ribbon or foil. Although widely used to produce small quantities of material for research purposes, the technique has seen little commercial application, for reasons related to the difficulty in scaling up the process, and in realizing stable operation.

The process is illustrated in Figure 1. A crucible contains molten material, and is positioned just above a rotating chill wheel. Upon application of an overpressure inside the crucible, molten material is ejected into

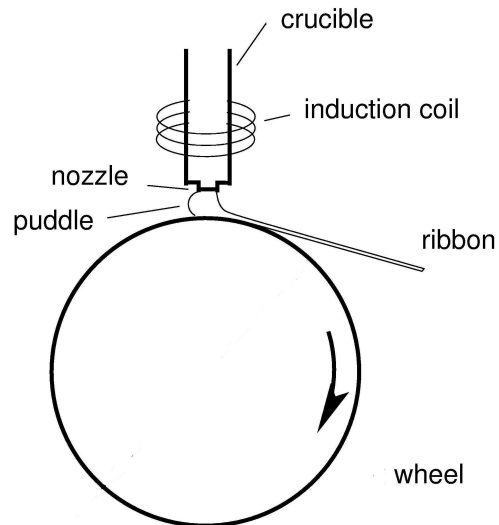


Figure 1: Schematic of a melt spinner (not to scale).

the very thin gap between the underside of the nozzle and the top of the wheel. For some part of the operating space of the process (defined by three parameters: the overpressure  $\Delta p$ , the gap height  $G$ , and the wheel speed  $U$ ), a so-called *puddle*, illustrated in Figure 2, will stabilize between the nozzle and wheel, with the inflow of melt balanced by the rate at which solidified ribbon is removed from the bottom of the puddle.

In a review paper by Steen and Karcher [3], the authors present an operability window (reproduced in Figure 3) as a function of two parameters driving the process: the overpressure and the wheel inertia, each non-dimensionalized by the surface tension of the melt that is responsible for containing the puddle within the gap. In this paper, we present the results of a two-dimensional model of the planar flow casting process, based on one developed previously [2], to examine this operability window numerically. Various

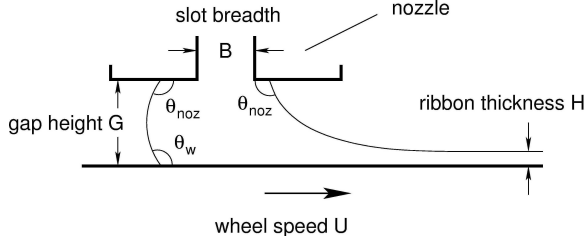


Figure 2: Close-up of a melt spinning puddle.

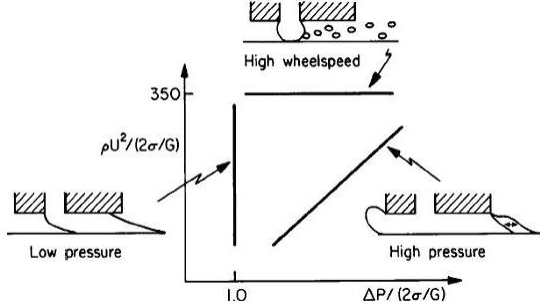


Figure 3: The operability window of Steen and Karcher [3].

improvements have been made to the previous model, but for the purposes of this paper, the significant difference is the boundary condition at the inlet to the puddle. Rather than a specified inflow rate, which is the boundary condition also applied in most previous modelling work, the results here are for a specified overpressure. The difference is significant: simulations for various specified inflow rates always yielded stable puddles [2]. On the other hand, as we will show in this paper, stable puddles formed only for a limited range of overpressures for a given wheel speed; above and below the range, simulations would not converge to a steady solution, with fluid configurations nowhere near what one would expect for stable operation.

## 2 METHODOLOGY

We present a brief overview of the model, similar to one developed previously and described in more detail in [2].

Our model of the planar flow casting process is based on the following assumptions: (i) a two-dimensional planar configuration, as the ribbon width and the wheel diameter are much greater than the gap height; (ii) incompressible, laminar, and Newtonian flow; (iii) the ribbon cools rapidly, so that solidification is to an amorphous (glassy) microstructure; (iv) the melt cools only to the wheel, and is characterized by a single

value of a heat transfer coefficient  $h$ ; (v) melt density  $\rho$ , surface tension  $\sigma$ , and thermal diffusivity  $\alpha$  are characterized by constant values; dynamic viscosity  $\mu$  is presumed to vary with temperature; and (vi) the process occurs within a vacuum, so that shear stresses at the free surface are zero, and the only flow is within the melt.

Equations governing flow and heat transfer from within the nozzle and gap are the equations of conservation of mass, momentum, and energy:

$$\nabla \cdot u = 0 \quad (1)$$

$$\frac{\partial u}{\partial t} + \nabla \cdot (uu) = -\frac{1}{\rho} \nabla p + \frac{1}{\rho} \nabla \cdot \tilde{\tau} + \frac{1}{\rho} F_{ST} \quad (2)$$

$$\frac{\partial T}{\partial t} + \nabla \cdot (uT) = \alpha \nabla^2 T \quad (3)$$

where  $u$  is velocity,  $p$  is pressure,  $T$  is temperature,  $\tilde{\tau}$  is the shear stress tensor, and  $F_{ST}$  is the surface tension force acting at the melt free surface, modelled as a body force according to the Continuum Surface Force approach of Brackbill et al. [1]. Note that we make no distinction between liquid and solid phases as the melt is assumed to solidify to an amorphous solid, and so releases no latent heat; thus, the flow equations are solved throughout the melt/solid. The flow “sees” the solidification via the temperature-dependent viscosity, which increases by several orders of magnitude as the melt cools.

The equations are discretized according to typical finite volume conventions on a rectilinear grid that encompasses the gap and 1 mm of the nozzle above the gap, and extends several millimetres both up and downstream of the exit of the nozzle, as illustrated in Figure 4. Velocities are defined normal to cell faces; scalar quantities including pressure and temperature are defined at cell centres.

The time discretization of equation 2 is via a two-step projection method: an interim velocity is calculated from the convective, viscous, and surface tension forces acting on the fluid during a timestep  $\Delta t$ . The convective and surface tension contributions are calculated explicitly, while the viscous term is treated implicitly. The interim velocity is then projected onto a divergence-free velocity field, which leads to an implicit Poisson equation for pressure. Finally, equation 3 is solved explicitly at each timestep following the pressure solve.

The free surface is represented via a volume-of-fluid approach: a scalar function  $f$  has a value of 1 within the fluid, and otherwise 0, and satisfies the advection

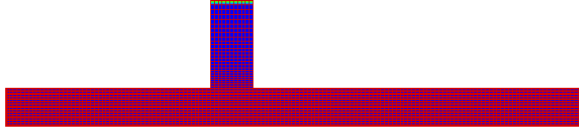


Figure 4: A sample mesh, that extends across the gap and 1 mm into the nozzle.

equation:

$$\frac{\partial f}{\partial t} + \nabla \cdot (uf) = 0 \quad (4)$$

In discretized form, the value of  $f$  corresponds to the volume fraction of cells filled with fluid, and so varies from zero to one, with the free surface located in cells with  $0 < f < 1$ . Equation 4 is discretized according to the method of Youngs [4], by reconstructing the interface at each timestep in a piecewise-linear manner, and then calculating flux volumes geometrically.

Initially, the simulation begins with fluid only in the top row of cells in the domain. A no-slip condition is imposed along the nozzle and wheel, with the wheel moving from left to right at the velocity  $U$ . There is no boundary condition at the upstream (left) side of the gap, as we halt simulations when fluid reaches this boundary. The downstream (right) edge of the domain is a simple outflow boundary, placed far enough downstream that ribbon usually has cooled sufficiently to be considered solid, and thus is moving at the wheel velocity.

Pressure is set to zero in any cells with  $f = 0$ , ie. in the vacuum surrounding the melt. At the top of the domain we prescribe an overpressure  $\Delta p$  rather than a specified inflow rate, as was done previously [2], and couple that to a zero gradient condition on velocity normal to the inlet. Note that we are not modelling the entire slot nozzle, which extends upward far more than 1 mm from the underside of the nozzle, but rather just the bottom part of it, and so presume that a fully developed profile exists at that point.

At the beginning of a simulation, as fluid first begins to enter the nozzle above the gap, it is the difference between the applied overpressure at the top of the domain and the zero pressure in the vacuum that drives flow; the velocity and volume fraction profiles are first uniform across the nozzle, but these quickly change to a rounded profile as the no-slip condition at the nozzle walls is imposed. By the time the fluid has filled the nozzle and is beginning to enter the gap, the velocity profile across the nozzle is nearly parabolic, with a small linear pressure gradient to offset viscous shear.

Finally, the surface tension calculation requires the

specification of a contact angle  $\theta$  at every triple point, as illustrated in Figure 2; these include the two points on the underside of the nozzle, where the up and downstream menisci meet the nozzle, and the point at which the upstream meniscus meets the wheel. The latter value matters little to the simulation, because at the wheel inertial and viscous forces dominate. But on the underside of the nozzle, the value will affect the position of the meniscus.

### 3 RESULTS

We begin by presenting results of a simulation that leads to the formation of a steady puddle. The same simulation was run on three different meshes and the results used to assess mesh-independence; the results presented here correspond to a mesh size of  $225 \times 90$  in the horizontal and vertical directions, respectively. The cells are uniformly distributed in the horizontal direction; in the vertical direction, the mesh is most refined at the bottom of the domain (at the wheel surface), and then gradually coarsens through the gap and into the nozzle.

All of the results in this paper are for material properties corresponding to molten Ni:  $\rho = 7870 \text{ kg/m}^3$ ,  $\sigma = 1.7 \text{ N/m}$ ,  $\alpha = 2.6 \times 10^{-5} \text{ m}^2/\text{s}$ , thermal conductivity  $k = 90 \text{ W/mK}$  (required to impose the heat transfer boundary condition at the wheel surface), and the following melt viscosity variation with temperature:

$$\mu = 1.66 \times 10^{-4} \exp \frac{2180}{T - 722} \text{ Pa} \cdot \text{s} \quad (5)$$

where  $T$  is specified in Kelvin.

The operating parameters for the first set of results are the following: gap height  $G = 0.375 \text{ mm}$ , nozzle slot breadth  $B = 0.5 \text{ mm}$ , wheel speed  $U = 26 \text{ m/s}$ , the heat transfer coefficient at the wheel  $h = 1 \times 10^6 \text{ W/m}^2\text{K}$ , and an overpressure  $\Delta p = 10 \text{ kPa}$ .

A contact angle  $\theta = 130^\circ$  was specified along the inside and underside of the nozzle, which is different than the  $170^\circ$  used previously [2]. We know from experiment that the melt is very non-wetting, but wonder whether the value may not be as high as we previously thought. A contact angle of  $\theta = 90^\circ$  was imposed along the wheel; we have no experimental basis for choosing this value, but do know that it matters little to the results.

Figure 5 illustrates the formation of a steady puddle. By 0.5 ms, the melt has filled most of the nozzle above the gap, and the profile at the front is rounded, reflecting both the no-slip condition and the non-wetting contact angle applied at the nozzle walls. At 1 ms, the

puddle has already begun to take shape: a rounded upstream meniscus, and a downstream meniscus that extends from the nozzle down to solid ribbon being pulled from beneath the puddle. Another ms later, the puddle has filled out: the upstream meniscus has moved upstream of the nozzle slot, while the downstream meniscus, although still pinned at the slot, has grown considerably longer. And as the last of the profiles of Figure 5 illustrates, the puddle at 2 ms is very near steady state, as the puddle at 10 ms looks very similar.

The steady state position of the menisci in Figure 5: upstream of the nozzle slot and pinned at the downstream end, is similar to results obtained previously [2] for specified melt inflow rates. Yet the downstream position is peculiar, as the little experimental evidence that exists suggests that both menisci move away from the nozzle, up and downstream. That was the rationale for lowering the contact angle from  $170^\circ$  to  $130^\circ$ , yet that change influences the position of the upstream meniscus much more than the downstream. It isn't clear at this point what would consistently lead to a downstream meniscus that is not pinned at the nozzle slot.

Figures 6 and 7 illustrate the variation of pressure vertically through the center of the nozzle and along the base of the puddle, respectively, for the steady puddle of Figure 5. Figure 6 illustrates the small pressure gradient required to drive fluid through the nozzle, and then the very large jump in pressure that occurs in the puddle, in reaction to the wheel pulling fluid from left to right. Along the wheel, in the vicinity of the nozzle, one sees the same jump in pressure, with a maximum just to the right of the nozzle centerline.

Figures 8 and 9 present results for overpressures lower and higher than the 10 kPa value that leads to a steady puddle, and the results change dramatically from the steady state. For too small an overpressure,  $\Delta p = 5$  kPa, the fluid within the gap never settles down to anything that resembles a steady puddle. Off and on, fluid does push upstream, and as evidenced by the profile at 8 ms, at times there is much fluid downstream. In the third of the contours, at 12 ms, one can see a large chunk of fluid exiting the domain at the right. Suffice to say that the entire simulation was characterized by incomplete wetting on the underside of the nozzle, and irregular upstream meniscus shapes. We ran the same simulation on other meshes and obtained similar overall behaviour, although the specifics varied considerably. We also ran the simulation presented in Figure 8 well past 10 ms, but the fluid configuration continued to change abruptly at various times.

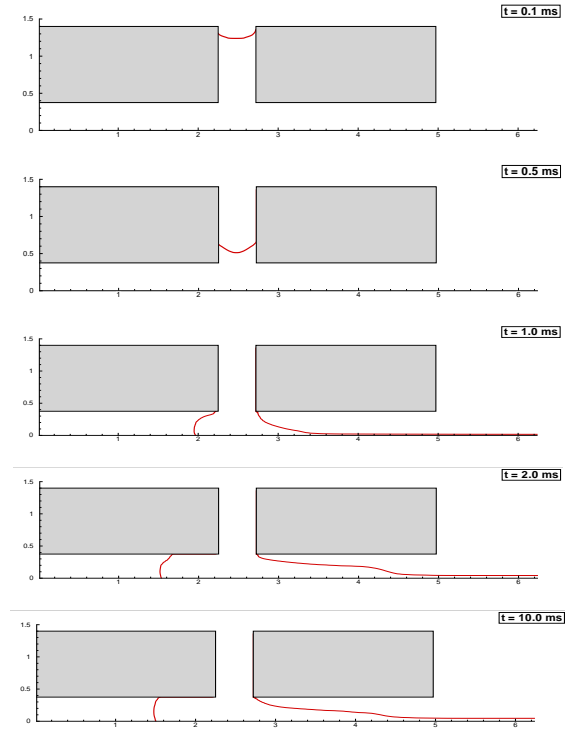


Figure 5: Free surface contours leading to the development of a stable puddle at the reference overpressure  $\Delta p = 10$  kPa.

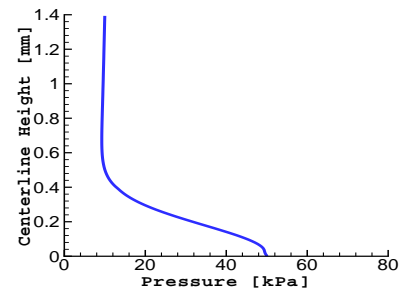


Figure 6: Pressure vertically through the center of the nozzle, for the puddle illustrated in Figure 5.

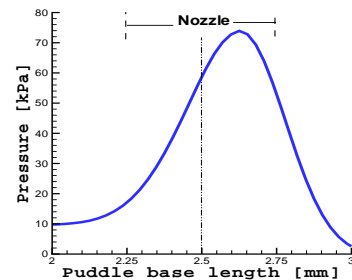


Figure 7: Pressure along the bottom of the puddle, for the puddle illustrated in Figure 5.

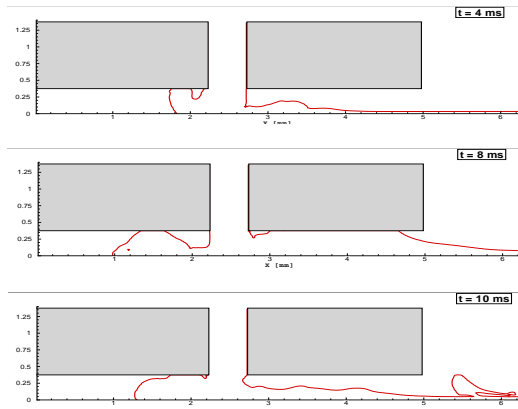


Figure 8: Puddle contours at 4, 8, and 10 ms, for  $\Delta p = 5$  kPa.

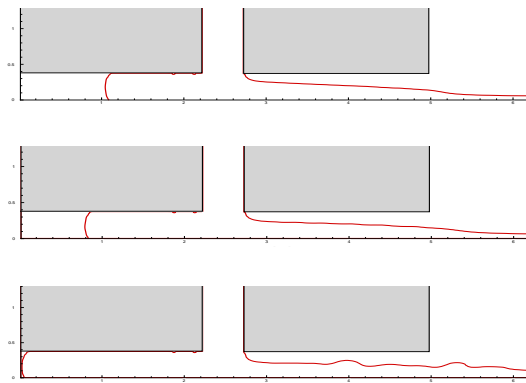


Figure 9: Puddle contours at 5, 10, and 20 ms, for  $\Delta p = 15$  kPa.

At too high a pressure (Figure 9), the result is smoother than for too low a pressure, but the puddle fails to reach steady state for a very different reason. In this case, as is also pictured in the cartoon at the right of the operability window (Figure 3), the pressure is simply too high, and so forces fluid all the way to the upstream end of the nozzle. In our case, we defined the end of the computational domain at that point, and stopped the simulation when fluid reached the left edge. Also, at 20 ms, note that waves have appeared on the downstream meniscus, that originate from the nozzle slot and travel towards the right. The reason for the waves, whether physical or numerical, is not known.

Figure 10 presents inflow rates versus time for the three simulations. At  $\Delta p = 10$  kPa, the rate is steady within a couple of ms of the beginning of the process. At 15 kPa, the inflow rate steadily increases with time, as the upstream meniscus moves left. And at 5 kPa, inflow rate fluctuates dramatically, and never reaches any semblance of steady state. Figure 11 presents a similar picture, but from the outflow end of the domain. Rib-

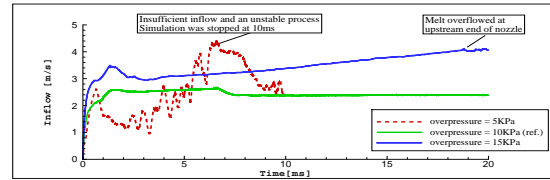


Figure 10: Inflow rate as a function of time, for the three different values of  $\Delta p$ .

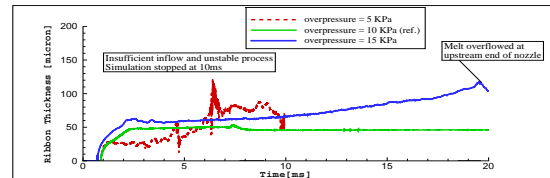


Figure 11: Ribbon thickness leaving the domain, as a function of time, for the three different values of  $\Delta p$ .

bon thickness  $H$  is plotted versus time, and again, the results for  $\Delta p = 10$  kPa are steady within a couple of ms (note that at steady state, inflow rate and outflow rate  $H * U$  are equal), at 15 kPa, the ribbon thickness grows with time, and at 5 kPa, there is no evidence of steady behaviour.

To conclude, the results of the effect of varying the overpressure are in qualitative agreement with the operability window of Figure 3, and are results that were not obtained when specifying a fixed melt inflow rate [2].

We also ran a series of simulations with an overpressure  $\Delta p = 10$  kPa, varying the wheel speed about the reference value of 26 m/s, in order to investigate operability behaviour along the vertical axis of Figure 3. Unlike the results already shown, we saw no sign of instability, but rather obtained a steady state solution for each  $U$ , as illustrated in Figure 12. In this case, the position of the upstream meniscus varies little over a wide range of wheel speeds; the significant differences are in the shape of the puddle downstream of the nozzle. Note too that ribbon thickness increases dramatically as the wheel speed decreases, and that in some cases, the ribbons are very thick, and for these the outflow boundary may not be positioned far enough downstream. Nevertheless, for each wheelspeed we obtained steady results, and the reason is not clear. One possible explanation is that the instability at high wheel speeds, illustrated in Figure 3 affects the depth of the puddle and ribbon, the dimension that we are not modelling with our two-dimensional approximation.

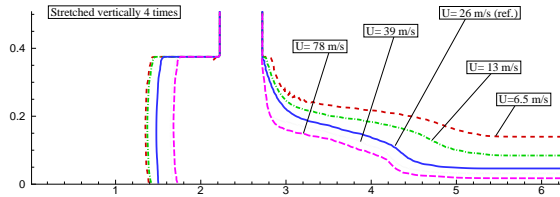


Figure 12: Steady puddle contours at five different wheel speeds, for  $\Delta p = 10$  kPa.

## 4 CONCLUSIONS

Unlike the results of most previous models of the planar flow casting process, this paper presents results for specified overpressure in the crucible. The change in boundary condition leads to quite different behaviour of the puddle formation process. In particular, the model demonstrates unstable puddles both for overpressures that are too small and too large. On the other hand, a series of simulations that examined the effect of varying the wheel speed at a given overpressure all led to stable puddles with no sign of instability, a result that may suggest that the instability at high wheel speeds occurs across the depth of the puddle, and so cannot be predicted with a two-dimensional code.

## REFERENCES

- [1] J. Brackbill, D. Kothe, and C. Zemach. A continuum method for modeling surface tension. *Journal of Computational Physics*, 100(2):335–354, 1992.
- [2] M. Bussmann, J. Mostaghimi, D. Kirk, and J. Graydon. A numerical study of steady flow and temperature fields within a melt spinning puddle. *International Journal of Heat and Mass Transfer*, 45(19):3997–4010, 2002.
- [3] P. Steen and C. Karcher. Fluid mechanics of spin casting of metals. *Annual Review of Fluid Mechanics*, 29:373–397, 1997.
- [4] D. Youngs. Time-dependent multi-material flow with large fluid distortion. In K. Morton and M. Baines, editors, *Numerical Methods for Fluid Dynamics*, pages 273–285. Academic Press, New York, 1982.